Building and Environment 226 (2022) 109731

Contents lists available at ScienceDirect

Building and Environment

journal homepage: www.elsevier.com/locate/buildenv

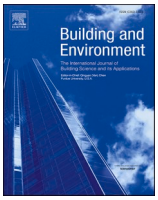

Monitoring of the effect of solar radiation and rain on the building envelope with integrated vertical vegetation

Elvira Nicolini [a,*], Maria Luisa Germanà [a], Giulia Marcon [b], Marcello Chiodi [c], Álvaro Gutiérrez [d], Francesca Olivieri [e]

[a] Department of Architecture, University of Palermo, Viale Delle Scienze Ed. 14, 90128, Palermo, Italy
[b] Department of Engineering, University of Palermo, Viale Delle Scienze Ed. 7, 90128, Palermo, Italy
[c] Department of Economics, Business and Statistics, University of Palermo, Viale Delle Scienze Ed. 13, 90128, Palermo, Italy
[d] ETSI Telecomunicación, Universidad Politécnica de Madrid, Av. Complutense 30, 28040, Madrid, Spain
[e] ETS de Arquitectura de Madrid, Universidad Politécnica de Madrid, Av. de Juan de Herrera, 4, 28040, Madrid, Spain

ARTICLE INFO

Keywords:
Green wall systems
Comfort
Passive retrofit
Nature-based solutions

ABSTRACT

The goal of the present paper is the verification of the improvement of the performance of a building envelope with a green wall also in conditions of high irradiance (≥0.6 kW/m^2) and with variable meteorological conditions (sunny, cloudy, and rainy), with a focus on intense rainfall and tempest. The object of the analysis has been the Innovation and Technology for Development Center in the University Campus of the Polytechnics of Madrid, where a modular system of integrated vertical vegetation has been installed on the skin of the South and West prospects. The study is based on the analysis of the effective thermoregulation capacity of the system in different climatic situations and has been allowed by a database covering a 3-year period, which contains data from continuous monitoring of the meteorological variations and thermal flows through a weather station and sensors placed on the external surface of the envelope, and on the external and internal surfaces of the wall. The experimentation shows that the use of a green wall on the West prospect is even more valid in conditions of high irradiance, as it allows reducing the temperature of the wall by 10 °C, compared to the scenario without the green wall. The combined effect of rain and solar radiation produces different results on the exposure of the walls, with a visible effect only on the South side.

1. Introduction

Nature-based solutions are compatible with retrofit interventions on existing buildings thanks to their characteristics of minimum intervention and reversibility, as their natural processes provide the envelope with a performance improvement regarding the indoor comfort in the building. In general, they represent easily mountable and unmountable solutions, as they are dry-placed, independent of the support, adaptable, and modulable. Moreover, the technique of plant pre-cultivation allows obtaining instant covering also on large surfaces.

Many studies show that nature-based solutions produce human well-being and environmental benefits, as they allow improving air quality through the deposition of polluting particles on leaves, hence reducing their atmospheric dispersion [1–4]. For this reason, they are especially advantageous in dense urban environments, as they protect the community from the exposition of UFPs (ultrafine particles) produced by vehicular traffic.

Green walls can also serve as natural thermal regulators, and so contribute to the improvement of urban microclimate both inside and outside buildings, balancing the high temperatures reached because of climate change [5,6]. The insulating effect is related to the different compositions of the systems, among which the presence of the support layer and intermediate air cavities, if present, which can be closed or open depending on whether the desired effect is traditional insulation or behavior like a ventilated façade.

The literature shows the capacity of the green walls to screen the building envelope, with a consequent reduction of the superficial temperature of the external wall of the building by up to 15 °C on the South-West side [7] and by up to 8 °C in the air cavity between the green skin and the wall [8], and indoor constant cooling by 2 °C [9].

Thermoregulation occurs through the water vapor exchange between vegetation and the atmosphere, thanks to the combined effect of

* Corresponding author.
E-mail address: elvira.nicolini@unipa.it (E. Nicolini).

https://doi.org/10.1016/j.buildenv.2022.109731
Received 25 July 2022; Received in revised form 17 October 2022; Accepted 20 October 2022
Available online 26 October 2022

plant transpiration from surface of leaves and evaporation from growing substrate [10]. In this way, in addition to increasing the efficiency of the thermal inertia of the building envelope, the green walls improve the ecological and environmental footprint of the constructions and the surrounding urban environment: one of the best-known effects is the contribution to the reduction of the heat island effect, with reductions of environmental temperature by up to 5 °C (UHI) [11–13].

Some studies on the effectiveness of green walls focus on the response to solar radiation, showing that at peak times the temperature difference between the wall with and without the green wall reaches 20 °C, while on cloudy days the temperature difference is reduced to 1–2 °C [14,15]. When building façades are exposed to sunlight radiation, cooling occurs because 5–30% of the solar energy hitting the leaf is reflected, 5–20% is used for photosynthesis, 10–50% is transformed into heat, 20–40% is used for evapotranspiration, and 5–30% passes through the leaf [16,17].

In terms of façade orientation, the vegetal layer is particularly effective in cooling East and West façades when they are exposed to maximum irradiance levels and should be considered with the same importance as the South orientation [18]. Analyses show that, in spring and summer, both shading values and the superficial temperature of the walls of the building skin confirm the great capacity of the green wall to intercept solar radiation, with a 71% reduction for the East façade and a 57% reduction for the West façade, compared to the skin without the green wall [19]. If there is an intermediate space between the green wall and the wall, the resulting microclimate is characterized by lower temperature and higher humidity [20].

McPherson has carried out a simulation with the software Shadow Pattern Simulation (SPS) to test the effects of solar radiation in similar residences located in various USA climates. Modeling has proven that the reductions in solar radiation absorption produced by the green wall increase yearly heating costs in cold climates by 28% and reduce cooling costs in hot climates by 61% [21].

Overall, the examined research works do not consider extreme and combined meteorological variations (rain, tempest, wind), when present. However, it is important to highlight the analysis of the behavior of green walls requires considering multiple variables, among which the variations of meteorological conditions, which can influence the real contribution to the performance of the envelope. In fact, in addition to the usual effect of the climate on the thermal performance of a building, it is also necessary to consider the variations related to the growth of the plants (density of the leaves, height of the plants, etc.) and their physiological response (transpiration, position of the leaves, etc.) as a function of atmospheric agents [22]. In general, most of the finished and ongoing research activities tend to draw their conclusions on experimental data from monitoring or simulations, with short verification periods and a focus on the spring-summer period [16,18–20]. This does not include the knowledge of the behavior of the green wall in other seasons, but this condition is necessary for the study of the global thermal balance of the building [23]. Moreover, most of the consulted studies are set in a temperate climate area in Europe and Asia [22], and short monitoring periods do not allow assessing the real response of the wall to extreme climate conditions, which are more frequent in the rest of the world and are expected to occur more often in temperate regions, due to climate change. The study presented in this contribution, despite being performed in a temperate climate, is based on continuous monitoring, carried out for a 3-year period. The extensive monitoring period has allowed verifying the behavior of the green wall also in rare conditions for temperate climates, which however are frequent in subtropical climates, for example. In particular, we have focused on variable weather conditions (sunny, cloudy), high radiation, intense rainfall and storms, and radiation-rain combinations, reflecting on the difference in the behavior of the building envelopes between areas with the green wall and those without it. Moreover, as of now, the state of the art does not show studies referred to the continuity in the effectiveness of the green wall under rain conditions, while it is an emerging theme for green roofs, which instead have proven good capacity of rainwater tightness, and a contextual reduction in the thermal load on the buildings [24].

2. Methods and data

2.1. The prototype

The object of the study consists of some rooms of the Innovation and Technology for Development Center (itdUPM) in the Moncloa Campus of the Polytechnic University of Madrid (UPM), where, a modular system of vegetal façade, called BIOFIVER, which has already been patented and commercialized, has been placed on the South, East, and West façades (Fig. 1). The real-time monitoring of the variation of external parameters and thermal flows during daytime and nighttime has allowed analyzing the effects of passive thermoregulation capacities with different meteorological situations, through a database built over a 3-year period (from 2016 to 2019). The itdUPM building hosts an interdisciplinary center, which integrates the various research lines in the fields of technology and sustainable development, and is provided with teaching spaces, meeting rooms, and laboratories. The building has been subjected to an energy retrofit in 2016 and has been realized with the goal of achieving quasi-zero energy consumption. The envelope is constituted by a load-bearing brick wall, cladded with a perforated aluminum profile anchored on L-shaped profiles. Between the wall and the perforated profile is a 20 cm air cavity. For the improvement of thermal transmittance, a layer of glass wool has been later added to the interior of the existing walls, while a green wall has been applied to part of the West, South, and East walls. The installed green wall is a 50*50*10 cm modular system and covers 11.25 m^2 on the South façade, 6.25 m^2 on the East, and 10 m^2 on the West one. The modular system consists of two tridimensional polypropylene frames, separated by a hydrophilic felt layer, while the front structure is infilled with an enriched organic substrate to allow the cultivation of plants. These have been selected according to their adaption to the specific climate context. The system is provided with a bleeding irrigation system, which allows uniform water supply on the whole surface.

In order to monitor the efficiency of the green wall, a system of sensors has been installed on the West and South walls, which recorded the temperatures on the skin and the wall, with and without the green wall, and on two different orientations, South and West. The sensors have been located on the external surface of the skin and on the external and internal surfaces of the wall. For the collected data, a minute-by-minute resolution was calculated as the mean of the values detected every 10 s in each node of the connected monitoring system. In particular, each node is connected to 8 Type T thermocouples, allowing a resolution of 0.1 °C, 3 pyrometers with 0.1 W/m^2 resolution and a weather station.

The monitoring system is based on an embedded system connected through an RS-485 serial bus to several distributed nodes. Every 10 ms each node obtains information from all the sensors at which it is connected. Every second the monitoring node performs the mean of the last 100 measurements and stores it internally to be acquired by the main controller through an RS-485 RTU-Modbus protocol; the main controller is based on an embedded Linux operating system and the data are registered on an internal SD card. It is made of a microcontroller with a UPS system and an electronic carrier to connect to the nodes. This information is stored together with the date and time. Moreover, every 5 min the main controller sends the data stored to the monitoring server. The monitoring server oversees synchronizing all data, performing all conversions from electrical to physical measurements and running periodic scripts which process the data and upload them to the monitoring database. The time series data set is currently composed by more than 2 million, from June 2016 until September 2019. The data are available for consultation on the link http://monitoring.robolabo.etsit.upm.es/itd/monitoring.php.

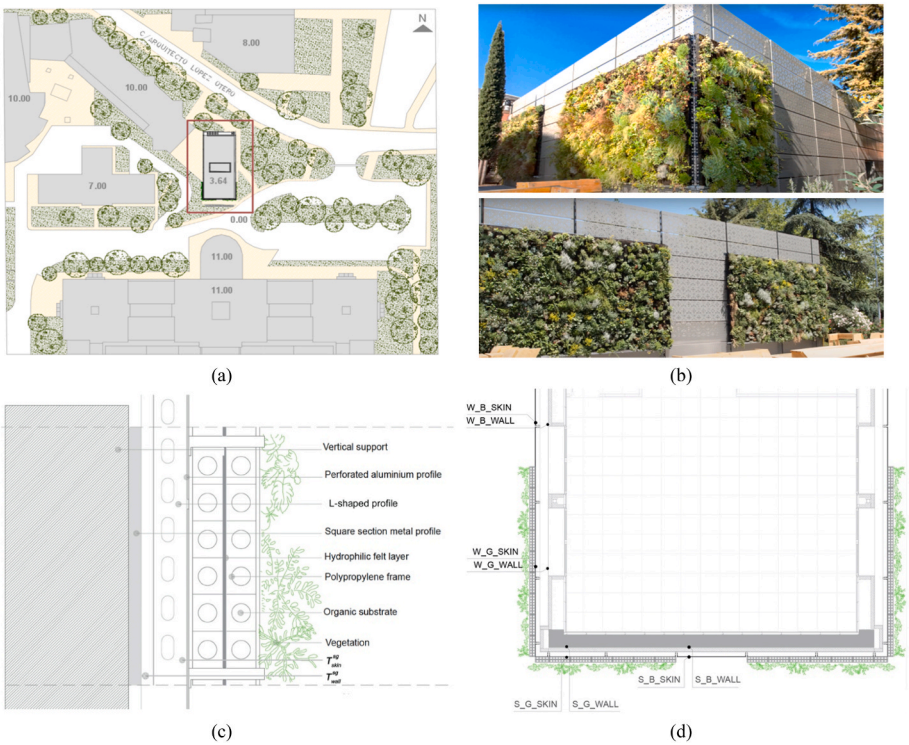

Fig. 1. Building of the Innovation and Technology for Development Center (itdUPM), located in the Moncloa University Campus of the Polytechnic School of Madrid (UPM); (a) General planimetry (Source: Image processing by Elvira Nicolini); (b) green wall on East and South walls (Images of idtUPM. Source: https://www.itd.upm.es/); (c) Section of the green wall (Source: Image by Valentina Oquendo); (d) Placement of the sensors on the West and South façades (Source: Image processing by Joaquin Sicilia Asociados). (For interpretation of the references to colour in this figure legend, the reader is referred to the Web version of this article.)

2.2. Smoothing conditional means and time series

The analysis of the relationship between multiple variables, such as the combined effect of rain and solar radiation on temperature differences, was carried out through visualization of *smoothed conditional means* through the ggplot2 package [25]. In particular, *loess regression* [26,27] is a non-parametric technique that uses *locally weighted regression* for the local estimation of a regression function. In this way, it is possible to identify non-linear trends, which would have otherwise been poorly evident if parametric linear or polynomial global models had been used.

Data on temperature differences measured by the sensors placed on the wall with and without the green wall (ΔT), for each orientation, have been modeled as a time series through ARMA(p, q) models [28] in the form:

$$X_t = \alpha_1 X_{t-1} + \ldots + \alpha_p X_{t-p} + \varepsilon_t + b_1 \varepsilon_{t-1} + \ldots + b_q \varepsilon_{t-q}$$

where p is the order of the autoregressive (AR) terms and q is the order of the moving average (MA) terms. These models are useful to describe time series when a given phenomenon appears to be influenced by its own determination in relation to p previous terms, through autoregressive terms and the linear combination of the ε_t errors at the previous instants. In this work, we considered one of its generalizations, known as ARIMA(p, d, q)(P, D, Q)$_m$ model with a seasonal component [29,30]. Hence, in addition to AR and MA terms, we considered a differentiation of the original series to fulfill the stationarity of the series and added seasonal terms expressing the *backshifts* of the season.

Hence, our goal is to express the two time series ΔT_S e ΔT_W (see Notation list below) through a seasonal ARIMA model as a function of autoregressive terms, moving averages, and the time series of the meteorological data, that is external temperature, rain, and irradiance as additional explanatory variables.

We deemed that minute-by-minute resolution was excessive; hence, the model has been evaluated through hourly data by calculating the hourly mean of all the involved parameters. Hence, in this case, the choice of the model is strictly connected to the identification of the order, expressed by the number of AR and MA components, for both seasonal and non-seasonal components, and of the period, set at 24 in accordance with the grouping of the hourly data. All models have been estimated and evaluated dividing the dataset into training and validation sets, respectively. The final model has been chosen through a *stepwise* process, using the AIC (*Akaike Information Criterion*), to individuate the best model without excessively increasing the number of parameters. For the sake of brevity, all the intermediate results are not shown here. Finally, the validity of the model is assessed through both the significance of each parameter and residual analysis. In particular, the plot of the auto-correlation function (ACF) allows visualizing the auto-correlation of the series with itself in previous lags. The Auto-Correlation Function plot shows the comparison between the ACF of the original series and the one estimated by the chosen model. In a good model, auto-correlations must be near 0, or at most there can be non-significant components, that is they must be within confidence intervals. The results of the estimated model are here reported in the Results section, with a particular focus on the parameters of the explanatory variables, such as external temperature, rainwater, and irradiance.

2.3. Initial data

The monitoring and data collection system allowed building a database containing temperature and rain data for the period between June 2016 and February 2019, with a minute-by-minute resolution, for both South and West façades. In this way, it was possible to perform specific statistical analyses to study the effect of irradiance and rain by comparing both the different façades and the mitigation effect of the green wall on external temperature and changes in climatic conditions. All the analyses have been carried out through the *R* statistical software [31].

Before carrying out the analyses, it was necessary to clean the dataset from all the *outliers*, presumably caused by interference of electrical signals or sensor maintenance. In particular, all the records of temperatures above 1800 °C, negative rain altimetric levels, or irradiance values above 1.3 kW/m^2 have been removed. The final dataset consists

of around 1 million observations, containing the variables outlined in the following table, where, in addition to initial measurements, auxiliary variables were built on the base of the original data in order to improve the analysis of the interaction between solar radiation and precipitation effects.

Variable	Description
Date, Time	Date and Time of the measurement
$T_{S\_G\_Wall}$, $T_{S\_G\_Skin}$	Temperature of the Green wall and skin, respectively, measured on the South Side
$T_{S\_B\_Wall}$, $T_{S\_B\_Skin}$	Temperature of the Bare wall and skin, respectively, measured on the South Side
$T_{W\_G\_Wall}$, $T_{W\_G\_Skin}$	Temperature of the Green wall and skin, respectively, measured on the West Side
$T_{W\_B\_Wall}$, $T_{W\_B\_Skin}$	Temperature of the Bare wall and skin, respectively, measured on the West Side
T_e	External temperature
Precipitation	Maximum altimeter level of flow and storm precipitation (mm/h)
Irradiance	Irradiance level (kW/m^2)
Day Night	Binary variable indicating "Day" corresponding to the following hours and season (Autumn 06:00–20:00, Spring 06:00–20:00, Summer 05:00–21:00, Winter 07:00–18:00) and "Night" otherwise.

Notation list. Synthesis of the variables that can be obtained from the data set and of the auxiliary variables built from the original data to improve the analysis of the interaction between solar radiation and rainfall effects.

All the added variables were built by observing the graphic representations of the involved measurements; for example, the distinction between day and night is useful to compensate for daily irradiance variation.

Symbol	Description
G	Green Wall
B	Bare Wall
S	South Orientation
W	West Orientation
Wall	Position of the sensor on the external surface of the wall (see Fig. 1d)
Skin	Position of the sensor on the external surface of the building skin (see Fig. 1d)
ΔT	Temperature difference between Bare and Green wall for each orientation ($\Delta T_S = T_{S\_B\_Wall} - T_{S\_G\_Wall}$ and $\Delta T_W = T_{W\_B\_Wall} - T_{W\_G\_Wall}$ corresponding to South and West, respectively)
ΔT^*	Temperature difference between skin and wall, with respect to a specific wall (i.e. $\Delta T^B = T_{B\_Skin} - T_{B\_Wall}$ and $\Delta T^G = T_{G\_Skin} - T_{G\_Wall}$ corresponding to Bare and Green respectively)
ΔT^*_e	Difference between external temperature and wall, with respect to a specific wall (i.e. $\Delta T^B_e = T_e - T_{B\_Wall}$ and $\Delta T^G_e = T_e - T_{G\_Wall}$ corresponding to Bare and Green wall respectively)

Notation list. Synthesis of the acronyms, with their description, used for data processing.

3. Results

The elaboration of the data has provided a picture of the overall behavior during the 3-year period, for each season, for South and West orientations, and for both the typologies of building skin. In the first part, the data show the general behavior of the building skin with the green wall, compared to the one without its, analyzing superficial temperature on the wall, and the temperature differences between the skin and the wall, also with different values of external temperature. In the second phase, the effect of the wall has been analyzed by comparing superficial temperature only at daytime (06:00–18:00). High and low irradiance thresholds have been defined, to distinguish between the reaction of the wall to disadvantageous meteorological conditions, in order to isolate superficial temperatures on the wall and on the skin in particular circumstances. Finally, the behavior of the skin has been evaluated in variable meteorological conditions (cloudy, sunny, variable, and rainy), analyzing temperatures in situations of combined rain and irradiance.

3.1. Data processing

The behavior of the difference between the temperatures measured by the B_Wall (without the green wall) and the G_Wall (with the green wall) sensors, on each side, is illustrated in Fig. 2, in terms of density distribution with respect to every season. During the summer, the superficial temperature of the sensor placed in a point without the green wall is tendentially higher than the one placed in a point with the green wall. During the winter, temperatures are very frequently equal, or the superficial temperature is lower without than with the green wall. Similar phenomenon occurs on both sides, yet more accentuated in the winter and less in the summer in the South-West.

Fig. 3 shows ΔT^* time series over the whole 3-year period. In the South side, without the green wall (red), there is higher variability of the superficial ΔT and hence wider thermal ranges between the skin and the wall over the 3-year period. On the West side, ΔT is slightly lower (by 5 °C). With the green wall (green), there is higher uniformity between the skin and the wall, again.

Further analysis focus on the comparison to external temperatures, as shown in Fig. 4. During the summer, the ΔT between the external temperature and the superficial temperature measured by the sensor with the green wall is tendentially higher than when this is not present. During the winter, temperatures are frequently equal, or the superficial temperature is lower where there is no green wall, compared to where it is present. The phenomenon is similar in both sides, although it is less accentuated during the summer in the West side.

Furthermore, the scatterplots represented in Fig. 5 show that during the summer, when external temperatures reach even 40 °C, without the green wall, the difference values are around 0; hence, the wall absorbs all the external heat. Conversely, with the green wall, the differences are around 7 °C; this shows the mitigation effect of the green wall. The effect of the green wall is the same in each side, South and West, respectively.

In order to focus on the solar irradiance effect, different thresholds for High/Low irradiance level have been detected on the base of preliminary analysis and with respect to each season: fall 0.4; spring 0.6; summer 0.7; winter 0.14. Fig. 6 shows that the effect of the green wall is more evident on the South wall, in terms of lower temperatures with higher irradiance in every season, with the green wall. There is no really evident effect on the West wall, except a slight difference in the summer. Considering the differences of temperatures (see Fig. 7) ΔT^* is mainly null, with high irradiance, in presence of the green wall; otherwise, without the green wall, the superficial temperature on the skin is much higher than on the wall. With low irradiance, the phenomenon is the same, but less evident. Same conclusions can be drawn for each side.

The mitigation function of the green wall is even more visible with variable irradiance. A different categorization of data has been done by hour-based evaluation to detect constant irradiance (standard deviation of hourly irradiance <0.5) and variable irradiance (standard deviation of hourly irradiance ≥ 0.5). Fig. 8 shows that ΔT^* is much lower (by around 20 °C), than without the green wall. The difference between the two skin typologies is sensible also with constant irradiance.

In order to extend the analysis and considering the rain effect, the distribution of precipitation is illustrated in Fig. 9, for each season and divided into day and night hours. The joint effect of rain and solar irradiance is shown in Fig. 10. As rainfall increases, ΔT^G is always close to 0, while ΔT^B is strongly affected by rain since in daytime, as rainfall increases, during the summer T_{wall} is higher than T_{skin} and during the winter T_{wall} is lower than T_{skin}; in terms of comfort, it should be just the opposite. The poor precipitation does not affect the behavior; this can be seen in the proportional trend of the graphs. In the rainiest season, that is spring, the T_{wall} with the green wall is higher than the T_{skin}.

Atmospheric conditions, such as cloudy, sunny, variable and rainy have been categorized by a new variable with different thresholds of

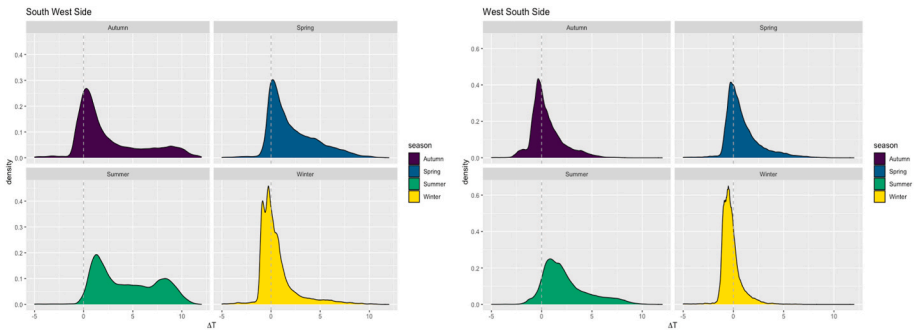

Fig. 2. ΔT density distribution by season. ΔT density distribution is proportional to the frequency of a given ΔT value over the 3-year period. It is expressed in °C and corresponds to the difference between the temperature values measured by the B_Wall (without the green wall) and the G_Wall (with the green wall) sensors on the South and West side, respectively. (For interpretation of the references to colour in this figure legend, the reader is referred to the Web version of this article.)

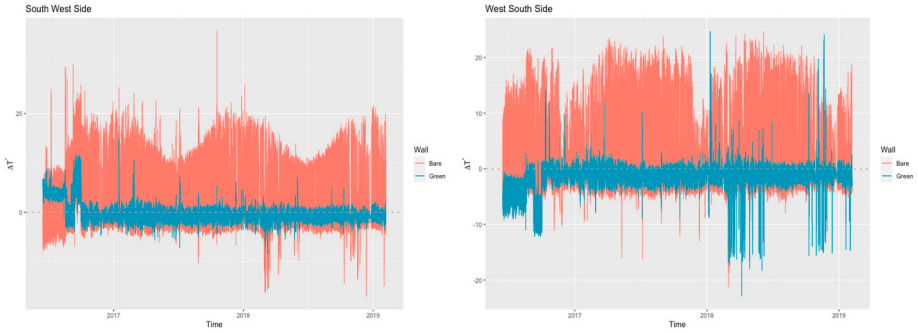

Fig. 3. ΔT* time series over the 3-year period. ΔT values, expressed in °C, are the difference between the temperature values measured by the Skin and Wall sensors on the South and West side, respectively.

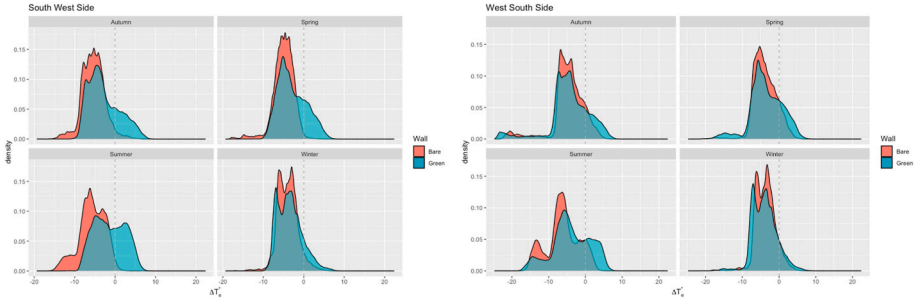

Fig. 4. ΔT^*_e distribution in every season. ΔT values, expressed in °C, are the difference between the temperature values measured by the B_Wall (without the green wall) and the G_Wall (with the green wall) sensors on the South and West side, respectively. (For interpretation of the references to colour in this figure legend, the reader is referred to the Web version of this article.)

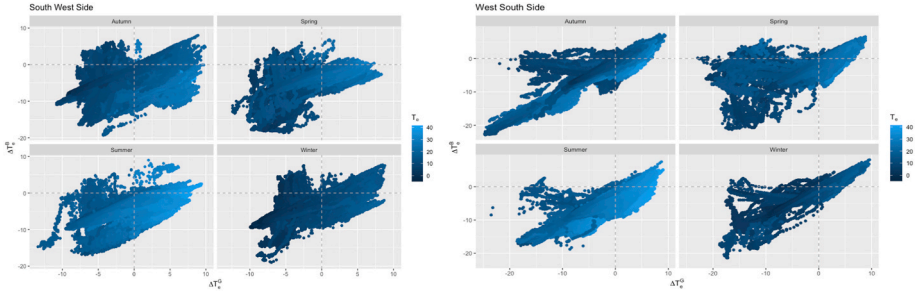

Fig. 5. ΔT^*_e comparison in every season as T_e varies. ΔT^*_e value, expressed in °C, is the difference between the external temperature value and the temperature value measured by the sensor on the each wall with and without the green wall (G and B, respectively). (For interpretation of the references to colour in this figure legend, the reader is referred to the Web version of this article.)

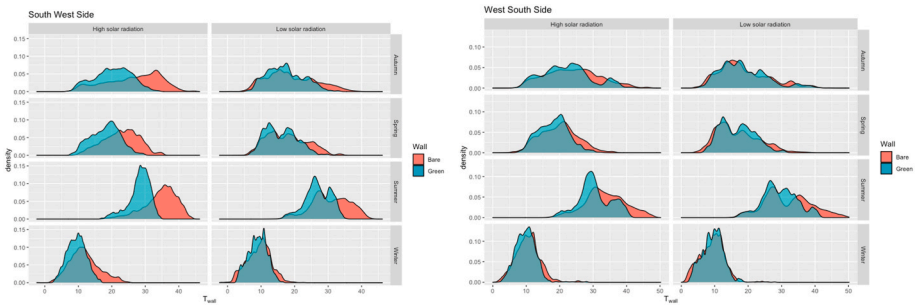

Fig. 6. T_{Wall} distribution in the daytime by irradiance in every season. The irradiance thresholds for the definition of High and Low are: fall 0.4; spring 0.6; summer 0.7; winter 0.14.

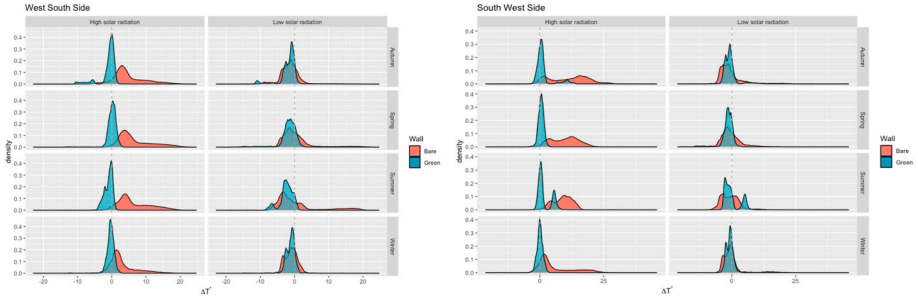

Fig. 7. ΔT* distribution in the daytime by irradiance every season.

Fig. 8. ΔT* distribution in the daytime by irradiance over the 3-year period, with respect to hour-based evaluation with constant irradiance (standard deviation of hourly irradiance <0.5) and variable irradiance (standard deviation of hourly irradiance ≥ 0.5).

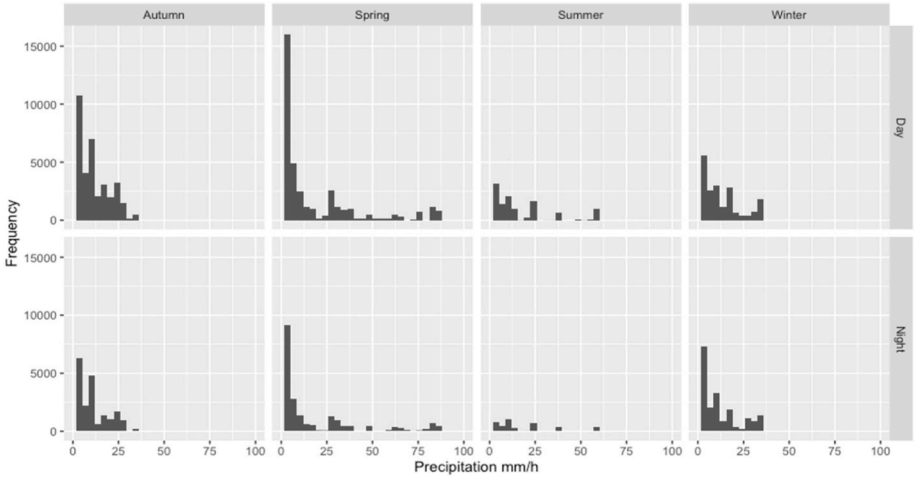

Fig. 9. Distribution of precipitation in every season, comparing daytime and nighttime.

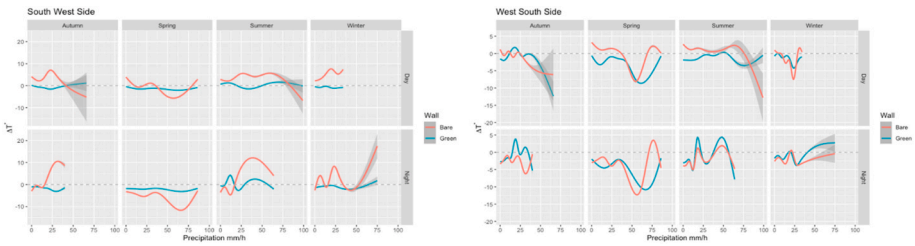

Fig. 10. Conditional mean ΔT* with increasing altimeter levels (mm/h) and presence/absence of Irradiance.

precipitation and irradiance:

	Maximum hourly precipitation	Standard deviation of hourly irradiance	Irradiance
Cloudy	0	<20	<0.02
Sunny	0	<20	≥0.02
Variable	0	≥20	
Rainy	>0		

Fig. 11 shows that all the points deviating from the bisector show temperature variation, depending on the presence/absence of the green wall. On sunny days, when irradiance is higher, the temperatures of the skin with the green wall appear to be higher than on the wall, by around 0–15 °C, with a concentration at around 5 °C, while without the green wall the differences between the skin and the wall are higher by more than 25 °C. On variable and rainy days, with high irradiance, there is a similar situation, but in several cases, the temperatures of the skin are lower than the wall; specifically, the ΔT^G is always around 5 °C, while without the green wall it increases up to 25 °C. On this wall, the variance in positive temperature differences without the green wall is even more evident, as irradiance increases.

A different point of view is given by Fig. 12: in the rainiest day, which occur is spring, with the most consistent rain stream and higher irradiance, T_{B_Wall} is higher than T_{G_Wall}, confirming that the green wall absorbs solar radiation. In the rainiest season, the spring, that is spring, with the most consistent rain stream and higher irradiance, T_{B_Wall} is often lower than T_{G_Wall}.

3.1.1. Analysis 1 – general conditions

The results confirm the insulating effect of the green wall, as the temperature difference between the wall without and with the green wall is around 2 °C in the winter (see Fig. 2). During the winter, the green wall manages to continuously cool the wall by showing temperature differences to 13 °C, compared to the skin without the green wall (see Fig. 2). The phenomenon is similar on both South and West façades, yet on the West one, it is less accentuated during the summer, while during the winter the insulating effect is more constant. Moreover, the overall analysis of the 3-year period shows that without the green wall the thermal difference between the skin and the wall is notable, up to 25 °C, while with the green wall the maximum difference is around 3 °C (see Fig. 3). With respect to external temperature, the contribution of the green wall is particularly sensible during the summer, more on the South than on the West façade, as it can cool the South wall by up to 10 °C, while on the West one by up to 7 °C (see Fig. 4). For example, considering multiple days with high temperatures (up to 40 °C), without the green wall, the wall absorbs all the external heat; conversely, the green wall can mitigate heat by around 7 °C (see Fig. 5).

3.1.2. Analysis 2 – focus on the effect of irradiance

In conditions of higher irradiance during the fall and the spring (irradiance ≥0.4 and ≥ 0.6 kW/m^2, respectively), the cooling of the skin with the green wall as a response to the high irradiance, is more present on the South wall (see Fig. 6). During the summer, the green wall has higher performance (compared to irradiance thresholds ≥0.7 kW/m^2), as it mitigates the temperature of the wall by around 10 °C, both South and West, suggesting that it would be particularly effective in tropical climates (see Fig. 6). This thesis is confirmed when examining the temperature difference between the skin and the wall. In fact, with the green wall, it is almost null, as plants manage to absorb notable irradiance. This is opposed to the behavior of the skin without the green wall, whose temperature grows by 25 °C more on the West façade and by more than 30 °C on the South one (see Fig. 7). The green wall is effective over the whole 3-year period, and the difference between the two typologies of skins is consistent in all seasons (see Fig. 8).

3.1.3. Analysis 3 – focus on the effect of rain

The rainiest season is spring (see Fig. 9). Rain streams up to 100 mm/h do not influence the behavior of the green wall on the South façade, whose inertia always prevents the destabilization of ΔT^G, which stays around 0. Conversely, the skin without the green wall strongly suffers the influence of rain (see Fig. 10), and this can be seen in the increase in temperature difference between the skin and the wall, to the disadvantage of thermal comfort (T_{Wall} increases in the summer and decreases in the winter). Instead, this behavior does not appear on the West façade, as apparently there is no relationship between temperature and increase of rain streams. However, in the spring, which is the rainiest season, the green wall still produces positive effects, as T_{wall} is always higher than T_{skin} (see Fig. 10).

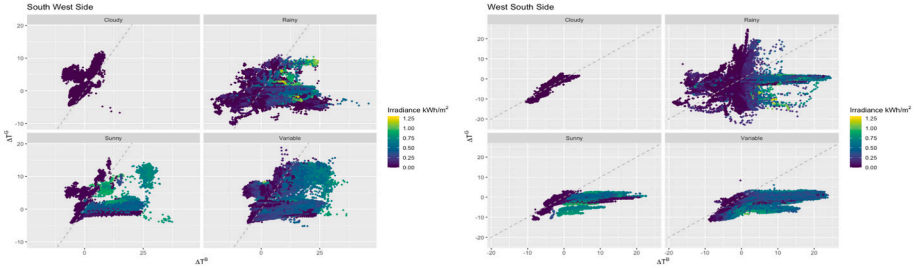

Fig. 11. ΔT* distribution by atmospheric events, with a focus on irradiance. ΔT* value, expressed in °C, is the difference between the temperature values recorded by the sensors on the skin and on the wall, on each side, with and without the green wall (G and B, respectively). (For interpretation of the references to colour in this figure legend, the reader is referred to the Web version of this article.)

Fig. 12. Scatterplot between ΔT and Irradiance (kW/m^2), with respect to increasing altimeter levels of precipitation (mm/h), during rainy morning days.

3.1.4. Analysis 4 – focused on the combined effect of rain and irradiance

On rainy days with high irradiance (≥0.6 kW/m^2), on the South façade, the temperature difference between the skin and the wall, with the green wall, is around 5 °C, while without the green wall it is around 25 °C (see Fig. 11). There is a difference between South and West: on the West façade, the behavior of the green wall changes between sunny days, on which ΔT^G is near 0, and rainy days, on which ΔT^G is around 15 °C. As stated before, the response to irradiance is always good, as ΔT^G is kept near 0. Without the green wall, also on the West façade, ΔT^B reaches 25 °C (see Fig. 11). The behavior of the wall also changes according to orientation, as also shown by the data related to the rainiest season, that is spring: on the West façade, unlike the South one, in some cases, T_{B_Wall} is lower than T_{G_Wall} (see Fig. 12).

3.1.5. Analysis 5 – analysis of time series

The ΔT temperature differences for both South and West orientations showed high variability. This required considering models with an oversized number of parameters, that is ARIMA(24, 1, 24)(1, 1, 1)$_{24}$. In addition to the parameters of the terms AR and MA, also the parameters describing the effect of the explanatory values resulted to be significant, except for the parameter related to the effect of rain on the temperature differences of the South wall. For the sake of brevity, only the final results are reported (see Table 3).

For completeness, here we report the residual analysis, by comparing the ACF plots of the original series and the residual values of the estimated model (see Figs. 13 and 14). The results show the presence of a cyclic component related to the dependency of temperatures to their own values in the previous hours. In particular, these correlations decrease up to 12 h before (hinting at the day/night effect, which interacts with irradiance level), then increase again with a peak in the value of the previous 24 h. The residuals of the model show no more significant auto-correlation considering previous lags, thus they are negligible because completely captured by the estimated model.

Table 3
The table reports, for each variable, the value of the estimated coefficient (Estimate), the standard error associated with the estimate (Std. Error), the value of the test statistic, obtained by testing the significance hypothesis of the Z parameter (Z value), and the respective p-value, which took lower values than the significance level 0.05, hence showing the empirical evidence in support of the statistical significance of the effect of the associated variable (significance detected '*').

ΔT	Variable	Estimate	Std. Error	Z value	p-value
ΔT_W	T_e	1.9028e-01	4.3455e-03	43.7885	<2.2e-16 *
	Irradiance	6.5787e-04	6.4263e-05	10.2371	<2.2e-16 *
	Precipitation	−2.0829e-02	3.3989e-03	−6.1282	8.89e-10 *
ΔT_S	T_e	0.25714838	0.00686603	37.4523	<2.2e-16 *
	Irradiance	0.00166693	0.00011149	14.9507	<2.2e-16 *
	Precipitation	0.00156694	0.00582168	0.2692	0.79

4. Discussion and conclusions

The results confirm the effectiveness of the green wall [6,7,16,18], as they show a better response to T_e throughout all the seasons both on the South and the West walls. This results in cooling the South wall by around 10 °C and the West wall by around 7 °C in the summer, and by insulating the skin in the winter, to the point of making T_{G_Wall} higher than T_e by around 9 °C, both on the South and the West walls. The difference between the two typologies of skins emerges especially in the summer, when T_{G_Wall} is lower than T_{B_Wall} by around 7 °C on the South façade, and by around 4 °C in the West; in the winter, an insulating effect appears, with T_{G_Wall} being 2 °C higher than T_{B_Wall} both on the South and the West façades. These data show the validity of the system for the reduction of the energy needs, especially considering the expected increase in average global temperatures from 2021 to 2040, between 1 and 2.5 °C [32]. This will in fact have a positive impact on the winter season but will produce fast overheating during the summer in hotter areas.

The response to solar radiation showing that on cloudy days the temperature difference is reduced (see Fig. 11) as also seen in previous studies [14,15].

For the South-European latitude, South screening is ideal, as this orientation has the highest number of hours of exposure to solar radiation; in the summer, solar radiation on the wall is not obstructed by horizontal overhangs, if present [33], due to its angle. On the West façade, there is a shadowed area in the morning, but strong solar radiation during the afternoon [34]. The data from our analysis show that screening the West wall is more valid in conditions of high irradiance, in which the performance of the green wall increases, and it can cool the wall by up to 10 °C less than the bare wall, and by 3 °C less than in normal conditions. Moreover, the skin tends to overheat (around 30 °C more than the wall) by transferring heat both to the wall and to the external environment, hence increasing the UHI phenomenon. In fall and spring, the response of the green wall to high irradiance is more consistent on the South wall. During the winter, the values of T_{G_Wall} in conditions of high irradiance have the same trend as in conditions of low irradiance; instead, T_{B_Wall} has higher values. In this specific case, the increase in T_{B_Wall} could allow the reduction in the use of mechanical heating in indoor environments in correspondence to the bare wall; however, the casualism of this condition could be disadvantageous, as it would require programming an active regulation system for indoor microclimate, while in values stay stable in spaces protected by the green wall. On the West façade, the green wall has good performance of thermal insulation, and the temperature difference between the skin and the wall is kept near zero in sunny, cloudy, and variable weather conditions.

Concerning rainfalls and the combined effect of rain and solar radiation, there is a different response according to the exposition of the wall. On the South façade, intense rain streams do not influence the performance of the green wall, unlike the bare skin, whose superficial temperature varies and leads to an increase and a diminution of T_{B_Wall}, respectively in the summer and in the winter. On the West façade, the behavior of the two typologies is similar and is not proportionally

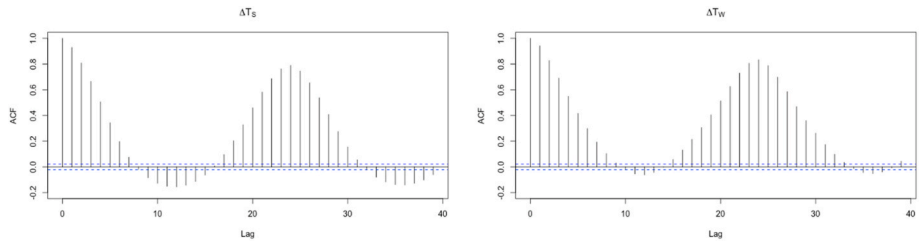

Fig. 13. Auto-Correlation Function (ACF) of the hourly series ΔT of temperature differences between bare and green, measured on the wall, with respect to different lags. (For interpretation of the references to colour in this figure legend, the reader is referred to the Web version of this article.)

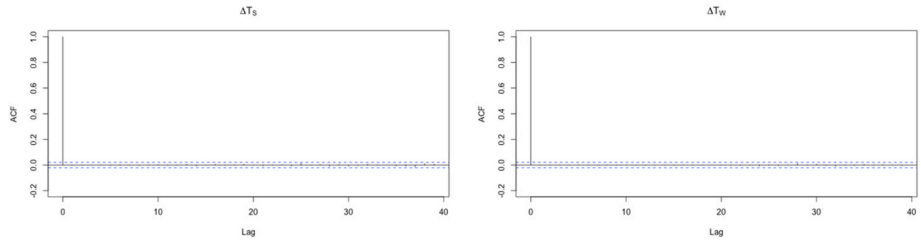

Fig. 14. Auto-Correlation Function (ACF) of the residuals of the model estimated on the hourly series ΔT of the temperature differences between bare and green, measured on the wall, with respect to different lags. (For interpretation of the references to colour in this figure legend, the reader is referred to the Web version of this article.)

affected by the increase in rain streams. The investigation of this last situation is being carried out through an ongoing analysis of the influence of dominant winds, and their combination with rain streams. The combination of rainfall and solar radiation shows leads to a continuous cooling effect only on the South side, together with a limited thermal difference between the skin and the wall, also with rain intensity above 100 mm/h and irradiance between 0.5 and 1 kWh/m^2.

The resulted limits of the green wall for the West orientation with intense rain streams could be considered negligible in a Mediterranean climate as in the investigated one, since the examination of the distribution of precipitation shows that this meteorological condition only appears in rare and sporadic cases, and mainly in spring. However, this information must be taken into account for rainy contexts, for which it could be opportune to consider overhanging technological solutions, aimed at shielding the façade from rain, to be activated manually or mechanically (also with sensors that detect the presence of rain).

CRediT authorship contribution statement

Elvira Nicolini: Writing – review & editing, Writing – original draft, Supervision, Resources, Project administration, Methodology, Investigation, Formal analysis, Data curation, Conceptualization. **Maria Luisa Germanà:** Writing – review & editing, Supervision, Conceptualization. **Giulia Marcon:** Writing – review & editing, Software, Methodology, Data curation. **Marcello Chiodi:** Writing – review & editing, Software, Methodology, Data curation. **Álvaro Gutiérrez:** Software, Data curation. **Francesca Olivieri:** Writing – review & editing, Supervision, Methodology, Data curation, Conceptualization.

Declaration of competing interest

The authors declare the following financial interests/personal relationships which may be considered as potential competing interests: Elvira Nicolini reports financial support was provided by European Social Fund PON AIM. Elvra Nicolini reports a relationship with University of Palermo that includes: employment.

Data availability

Data will be made available on request.

Acknowledgment

This research was funded by the Italian Ministry of Education, University and Research (MIUR) with the project PON “Research and Innovation 2014–2020” Section 1 “Researchers Mobility” with D.D. 407 of February 27, 2018 co-financed by the European Social Fund–CUP B74I19000650001–id project AIM 1890405–3, area: “Technologies for the Environments of Life”.

We acknowledge the itdUPM Institute (https://www.itd.upm.es/) and the Robolabo Robotics Laboratory (http://www.robolabo.etsit.upm.es/) for providing the data of the monitoring system; Professor Lorenzo Oliveri, for his contribution on sensors; Dr. Valentina Oquendo for providing the detail of the stratigraphy of the green wall (figure c) and contributing to drawing the floor plan of the building (figure d).

References

[1] J.J. Baik, K.H. Kwak, S.B. Park, Y.H. Ryu, Effects of building roof greening on air quality in street canyons, Atmos. Environ. 61 (2012) 48–55.
[2] J. Klingberg, M. Broberg, B. Strandberg, P. Thorsson, H. Pleijel, Influence of urban vegetation on air pollution and noise exposure–a case study in Gothenburg, Sweden, Sci. Total Environ. 599 (2017) 1728–1739.
[3] K. Perini, M. Ottelé, S. Giulini, A. Magliocco, E. Roccotiello, Quantification of fine dust deposition on different plant species in a vertical greening system, Ecol. Eng. 100 (2017) 268–276.
[4] M.Y. Lin, G. Hagler, R. Baldauf, V. Isakov, H.Y. Lin, A. Khlystov, The effects of vegetation barriers on near-road ultrafine particle number and carbon monoxide concentrations, Sci. Total Environ. 553 (2016) 372–379.
[5] R. Sendra-Arranz, V. Oquendo, L. Olivieri, F. Olivieri, C. Bedoya, A. Gutiérrez, Monitorization and statistical analysis of south and west green walls in a retrofitted building in Madrid, Build. Environ. 183 (2020), 107049.
[6] S. Aakriti, S. Takafumi, Evaluation of the suppressive effects on solar radiation for a building façade covered with green layers in the Kathmandu valley, Environ. Challange 5 (2021), 100246. ISSN 2667-0100.
[7] A.H. Block, S. Livesley, N.S. Williams, Responding to the Urban Heat Island: a Review of the Potential of Green Infrastructure, Victorian Centre for Climate Change Adaptation, 2012.
[8] G. Pérez, L. Rincón, A. Vila, J.M. González, L.F. Cabeza, Behaviour of green facades in Mediterranean Continental climate, Energy Convers. Manag. 52 (4) (2011) 1861–1867.

[9] T. Safikhani, A.M. Abdullah, D.R. Ossen, M. Baharvand, Thermal impacts of vertical greenery systems, Rigas Tehniskas Universitates Zinatniskie Raksti 14 (2014) 5.
[10] L. Kleerekoper, M. Van Esch, T.B. Salcedo, How to make a city climate-proof, addressing the urban heat island effect, Resour. Conserv. Recycl. 64 (2012) 30–38.
[11] N.H. Wong, A.Y.K. Tan, Y. Chen, K. Sekar, P.Y. Tan, D. Chan, N.C. Wong, Thermal evaluation of vertical greenery systems for building walls, Build. Environ. 45 (3) (2010) 663–672.
[12] A. Onishi, X. Cao, T. Ito, F. Shi, H. Imura, Evaluating the potential for urban heat-island mitigation by greening parking lots, Urban For. Urban Green. 9 (4) (2010) 323–332.
[13] E.A. Eumorfopoulou, K.J. Kontoleon, Experimental approach to the contribution of plant-covered walls to the thermal behaviour of building envelopes, Build. Environ. 44 (5) (2009) 1024–1038.
[14] U. Mazzali, F. Peron, P. Romagnoni, R.M. Pulselli, S. Bastianoni, Experimental investigation on the energy performance of Living Walls in a temperate climate, Build. Environ. 64 (2013) 57–66.
[15] E. Cuce, Thermal regulation impact of green walls: an experimental and numerical investigation, Appl. Energy 194 (2017) 247–254.
[16] A. Shrestha, T. Shimizu, Evaluation of the suppressive effects on solar radiation for a building façade covered with green layers in the Kathmandu valley, Environ. Challange 5 (2021), 100246.
[17] M. Ottelé, K. Perini, A.L.A. Fraaij, E.M. Haas, R. Raiteri, Comparative life cycle analysis for green façades and living wall systems, Energy Build. 43 (12) (2011) 3419–3429.
[18] M.K.A.M. Sulaiman, M. Jamil, M.F.M. Zain, Solar Radiation Transmission of Green Façade in the Tropics, Kongres Penyelidikan & Inovasi UKM2013, 2013.
[19] H.M.P.I.K. Herath, R.U. Halwatura, G.Y. Jayasinghe, Evaluation of green infrastructure effects on tropical Sri Lankan urban context as an urban heat island adaptation strategy, Urban For. Urban Green. 29 (2018) 212–222.
[20] G. Pérez, J. Coma, S. Sol, L.F. Cabeza, Green facade for energy savings in buildings: the influence of leaf area index and facade orientation on the shadow effect, Appl. Energy 187 (2017) 424–437.
[21] E.G. McPherson, L.P. Herrington, G.M. Heisler, Impacts of vegetation on residential heating and cooling, Energy Build. 12 (1) (1988) 41–51.
[22] G. Pérez, J. Coma, I. Martorell, L.F. Cabeza, Vertical Greenery Systems (VGS) for energy saving in buildings: a review, Renew. Sustain. Energy Rev. 39 (2014) 139–165.
[23] F. Olivieri, D. Redondas, L. Olivieri, J. Neila, Experimental characterization and implementation of an integrated autoregressive model to predict the thermal performance of vegetal façades, Energy Build. 72 (2014) 309–321.
[24] M.T. Simmons, B. Gardiner, S. Windhager, J. Tinsley, Green roofs are not created equal: the hydrologic and thermal performance of six different extensive green roofs and reflective and non-reflective roofs in a sub-tropical climate, Urban Ecosyst. 11 (4) (2008) 339–348.
[25] H. Wickham, Data analysis, in: ggplot2: Elegant Graphics for Data Analysis, Springer, New York, NY, 2016.
[26] W.S. Cleveland, Robust locally weighted regression and smoothing scatterplots, J. Am. Stat. Assoc. 74 (1979) 829–836.
[27] W.S. Cleveland, C. Loader, Smoothing by local regression: principles and methods, in: W. Härdle, M.G. Schimek (Eds.), Statistical Theory and Computational Aspects of Smoothing. Contributions to Statistics, Physica-Verlag HD, 1996, https://doi.org/10.1007/978-3-642-48425-4_2.
[28] G.E.P. Box, G. Jenkins, Time Series Analysis, Forecasting and Control Holden-Day, San Francisco CA, 1970.
[29] S.C. Hillmer, G.C. Tiao, An ARIMA-model-based approach to seasonal adjustment, J. Am. Stat. Assoc. 77 (377) (1982) 63–70, https://doi.org/10.1080/01621459.1982.10477767.
[30] T. Dimri, S. Ahmad, M. Sharif, Time series analysis of climate variables using seasonal ARIMA approach, J. Earth Syst. Sci. 129 (2020) 149, https://doi.org/10.1007/s12040-020-01408-x.
[31] R Core Team, R: A Language and Environment for Statistical Computing, R Foundation for Statistical Computing, Vienna, Austria, 2021. https://www.R-project.org/.
[32] H.O. Pörtner, D.C. Roberts, H. Adams, C. Adler, P. Aldunce, E. Ali, R. Ara Begum, R. Betts, R. Bezner Kerr, R. Biesbroek, J. Birkmann, K. Bowen, E. Castellanos, G. Cissé, A. Constable, W. Cramer, D. Dodman, S.H. Eriksen, A. Fischlin, Z. Zaiton Ibrahim, Climate Change 2022: Impacts, Adaptation and Vulnerability, IPCC, 2022. https://edepot.wur.nl/565644.
[33] M. Stanganelli, C. Gerundo, L'adattamento Delle Città Ai Cambiamenti Climatici, FedOA-Federico II University Press, 2018.
[34] G. Chiesa, J. von Hardenberg, Including Climate Change Time-Dimensions in Bioclimatic Design, TECHNE-Journal of Technology for Architecture and Environment, 2020, pp. 204–212.